Journal of Materials Chemistry C

Synthesis and Physical Properties of Layered Copper Oxytellurides $Sr_2TMCu_2Te_2O_2$ (*TM* = Mn, Co, Zn)

Journal:	*Journal of Materials Chemistry C*
Manuscript ID	TC-ART-09-2018-004506.R2
Article Type:	Paper
Date Submitted by the Author:	13-Oct-2018
Complete List of Authors:	Song, Dongjoon; Seoul National University Research Institute of Basic Sciences, Physics Guélou, Gabin; National Institute for Materials Science Mori, Takao; National Institute for Materials Science, Ochi, Masayuki; Osaka University Kuroki, Kazuhiko; Osaka University Fujihisa, Hiroshi; National Institute of Advanced Industrial Science and Technology, Gotoh, Yoshito; National Institute of Advanced Industrial Science and Technology, Iwasa, Yuki; National Institute of Advanced Industrial Science and Technology Tsukuba Center Tsukuba Central Eisaki, Hiroshi; National Institute for Advanced Industrial Science and Technology, Nanoelectronics Research Institute Ogino, Hiraku; National Institute of Advanced Industrial Science and Technology,

Journal Name

ARTICLE

Synthesis and Physical Properties of Layered Copper Oxytellurides $Sr_2TMCu_2Te_2O_2$ (*TM* = Mn, Co, Zn)

Received 00th January 20xx,
Accepted 00th January 20xx

DOI: 10.1039/x0xx00000x

www.rsc.org/

Dongjoon Song[a,b], Gabin Guélou[c], Takao Mori[c], Masayuki Ochi[d], Kazuhiko Kuroki[d], Hiroshi Fujihisa[a], Yoshito Gotoh[a], Yuki Iwasa[a], Hiroshi Eisaki[a] and Hiraku Ogino[*a]

We synthesized new series of layered copper oxytellurides $Sr_2TMCu_2Te_2O_2$ with variation in transition metal (*TM*= Mn, Co, Zn) elements. These compounds are the first example having alternately stacked anti-fluorite Cu_2Te_2 layer and perovskite-like *TM*-oxide layer. Reflecting the longer ionic radius of Te than Se and S, it exhibits larger lattice parameters than isostructural sulfides and selenides. First principle band structure calculation for the Zn compound as a representative, predicts a semiconducting direct band gap ~1.7 eV and Co compound shows comparable band gap in the diffuse reflectance measurement result. From the thermoelectric property study, we obtained power factor ~70 $Wm^{-1}K^{-2}$ and figure of merit *ZT* ~0.045 at 770 K for the Co compound, which encourages further improvement in thermoelectric response by applying various enhancement methods. For the magnetic property, signature of antiferromagnetic order is observed in the Co and Mn compound. The present results not only highlight the structural flexibility of the system to tune physical properties but also suggest that replacement of blocking layer can be a new direction to improve thermoelectric performance of layered copper oxychalcogenides.

Introduction

Mixing multiple anions and stacking different type of layers in single phase state has rather recently begun to be considered as a playground to explore new solid-state-materials and novel properties.[1] For instance, oxy-pnictides and -chalcogenides with alternately stacked fluorite and antifluorite layers have provided fascinating functionalities, such as high temperature superconductivity in *RE*FeAsO (*RE* = rare earth),[2-4] p-type transparent conductivity in LaCu*Ch*O (*Ch* = S, Se and Te),[5-7] and high thermoelectric figure of merit in BiCuSeO.[8-10] Moreover, the structural flexibility of the layered structure has offered fruitful opportunities to tune the functionality of the materials. *RE*FeAsO exemplifies that since the anti-fluorite iron-pnictide layer takes charge of superconductivity while its *RE* oxide layer plays a role of blocking layer and charge reservoir, modifying the structure of blocking layer have been intensively exploited to improve the functionality of the iron-based superconductor.[11-13]

As one of mixed anion hetero-layered system, series of $Sr_2Mn_3Sb_2O_2$ type compounds consisting of alternately stacked the antifluorite and perovskite-like transition metal (*TM*) oxide layers, namely perovskite-antifluorite,[14] have attracted interest because of their novel electric and magnetic properties.[15-21] In particular, $Sr_2TMCu_2Ch_2O_2$ which shares the antifluorite Cu_2Ch_2 layer with BiCu*Ch*O bears the potential to be a high thermoelectric material, because the high thermoelectricity of BiCuSeO is ascribed mainly to the property of its Cu_2Se_2 layer.[22] Indeed, good thermoelectric performance was reported in $Sr_2CoCu_2Se_2O_2$.[21] Besides, significant impact on magnetism by substitution of Alkaline Earth (*AE*) and *TM* elements, for example $(Sr,Ba)_2CoCu_2S_2O_2$ and $Sr_2(Mn,Co)Cu_2Se_2O_2$, respectively,[17,19] is also another notable feature of the perovskite-antifluorite copper oxychalcogenides.

Though the Cu_2Ch_2 layer of $Sr_2TMCu_2Ch_2O_2$ is regarded as the main conduction path, the compositional investigation of this layer has not been fully undertaken. Until now not only there is no compound with *Ch* = Te while many compounds have been reported for *Ch* = S and Se, but also systematic study on *TM* dependence has been rarely investigated. In this study, we explored layered perovskite-antifluorite copper oxytellurides with the variation of *TM* element. Three new compounds, $Sr_2TMCu_2Te_2O_2$ (*TM* = Mn, Co, Zn) were successfully synthesized by solid state

[a] National Institute of Advanced Industrial Science and Technology (AIST), Tsukuba 305-8568, Japan
[b] Center for Correlated Electron Systems, Institute for Basic Science, Seoul 151-742, Republic of Korea. E-mail: scdjsong@snu.ac.kr
[c] National Institute for Materials Science (NIMS), MANA, Tsukuba, 305-0044, Japan
[d] Department of Physics, Osaka University, Toyonaka, Osaka 560-0043, Japan.
† Electronic Supplementary Information (ESI) available: See DOI: 10.1039/x0xx00000x

reactions. Band structure calculation, which predicts semiconducting direct band gap ~1.7 eV, were carried out followed by the measurements on optical, transport, and magnetic properties. Thermoelectric performance estimated by figure of merit *ZT* reaches ~ 0.045 at around 770 K for *TM* = Co compound. These values in the pristine compound encourages further investigation on the potential of the layered perovskite-antifluorite copper oxytellurides as the high thermoelectric material.

Experimental

Chemicals and synthesis method

The $Sr_2TMCu_2Te_2O_2$ (*TM* = Mn, Co, Zn) samples were synthesized by solid state reaction. Cu (99.9%, Rare Metallic), Te (99.99%, Kojundo Chemical), Sr (99%, Kojundo Chemical), MnO_2 (99.9%, Furuuchi Chemical), Mn (99.8 %), Co (99.9%, Rare Metallic), Zn (99.9%, Furuuchi Chemical), and SrO powder were used as raw materials. Particularly, SrO was obtained from $SrCO_3$ (99.99%, Furuuchi Chemical) by 1200 °C heat treatment. Stoichiometric amount of the raw materials were mixed in an Ar filled glove box to prevent contamination from oxygen and moisture. The cold-pressed mixed powders were put into the silica tube or cubic anvil pressure cell to carry out solid reaction at 800~900°C under the evacuated environment for 1 day (*TM* = Mn, Co) or high pressure (2GPa) for 1 hour (*TM* = Zn), respectively. All the obtained phases are stable in the air at room temperature.

Characterization

The constituent phases are characterized by the powder X-ray diffraction (XRD) with RIGAKU Ultima IV. The XRD intensity data were collected in the 2θ range of 5–80° in steps of 0.02° using Cu-K_α radiation at room temperature. The lattice constants and the atomic positions were refined via Rietveld analysis using BIOVIA's Materials Studio Reflex software (version 2017 R2).[23] Chemical compositions were analyzed by using energy dispersive X-ray spectrometer (EDX); Oxford SwiftED3000 equipped with scanning electron microscope (SEM); Hitachi TM3000. Diffuse reflectance measurements were performed by Shimadzu UV-2600 spectrophotometer equipped with ISR-2600Plus. By using an ULVAC ZEM-2, electrical resistivity, Seebeck coefficient and thermal conductivity were measured on the pellets along the direction perpendicular to pressure applied for pelletization. The pellets with the density larger than 94 % were obtained from spark plasma sintering method except for $Sr_2ZnCu_2TeO_2$ having around 83% density, which was an as-gotten pellet from the cubic anvil-type high-pressure synthesis. Because of the tiny size of as-gotten pellet owing to the very small sample container of cubic anvil cell, it did not fit the instrumental standard and measurement on thermal conductivity of the Zn compound was inevitably skipped. The thermal conductivity was fitted with a polynomial function to calculate *ZT* as the measured electrical and thermal conductivity data points do not coincide at the same temperature (See Fig. S1 in Supplementary Information). Temperature dependence of magnetic susceptibility was measured by Quantum design magnetic property measurement system.

Band structure calculation

In first-principles calculations of $Sr_2ZnCu_2Te_2O_2$, we first determined the atomic coordinates by structural optimization using the Vienna *ab initio* simulation package (VASP).[24-27] The lattice constants determined by our experiment were used. In the structural optimization, we used the Perdew-Burke-Ernzerhof parametrization of the generalized gradient approximation (PBE-GGA)[28] with an inclusion of the spin-orbit coupling (SOC). After determining the crystal structure, we performed the band structure calculation using the WIEN2k package.[29] In the band structure calculation, we employed the modified Becke-Johnson potential[30,31] with an inclusion of SOC. The power factor was calculated with the Boltzmann transport theory using the BoltzTraP code.[32] Constant relaxation-time approximation was used here. In the same manner, we also calculated the power factor of BiCuSeO, while its crystal structure was taken from experiment[33].

Results and discussion

Figure 1a shows the result of Rietveld refinement of $Sr_2ZnCu_2Te_2O_2$. The simulated patterns are in good agreement with the obtained data. Structural parameters of the compounds are listed in Table 1. The main phase of this compound is formed under high pressure, about 2GPa, while ambient pressure synthesis does not work probably because of relatively large size mismatch of Cu-Te and Sr-Zn-O layer. The determined crystal structure of $Sr_2ZnCu_2Te_2O_2$ is shown in Fig. 1c and corresponds to the $Sr_2Mn_3Sb_2O_2$-type structure, space group *I4/mmm*, consisting of alternately stacked anti-fluorite type Cu_2Te_2 layer and square planar Zn oxide layer. Between these two layers, Sr surrounded by 4 tellurium and 4 oxygen forms the interstitial layer. To the best of our knowledge, the present compound is the first report of *Ch* = Te derivation in this system. The determined lattice constants of the compound are $a = 4.1715(1)$ Å and $c = 19.5983(2)$ Å. These values are much larger than those of related compounds such as $Sr_2ZnCu_2S_2O_2$ having $a = 4.0079(7)$ Å and $c = 17.7196(34)$ Å [12] reflecting larger ionic radius of Te^{2-} (2.21 Å) than S^{2-} (1.84 Å). In this compound, *TM* ions are surrounded by 4 in-plane oxygen and 2 apical chalcogen atoms resulting in a tetragonally elongated perovskite structure, providing a counterpoint to perovskite oxide phases such as the three-dimensional cubic perovskites $AETMO_3$ (AE = Alkaline Earth).

Table 1 Structural parameters for $Sr_2ZnCu_2Te_2O_2$ at room temperature

Atoms	*x*	*y*	*z*	Occupancy	U_{iso}
Sr1	0.0	0.0	0.4179(1)	1.0	0.015(1)
Zn1	0.0	0.0	0.0	1.0	0.015(1)

Cu1	0.0	1/2	1/4	1.0	0.015(1)
Te1	0.0	0.0	0.1660(1)	1.0	0.015(1)
O1	0.0	1/2	0.0	1.0	0.015(1)

Space group: *I*4/*mmm*
Lattice constant: a = 4.1715(1) Å, c = 19.5983(2) Å,
V = 341.04(2) Å^3
Zero point shift: Z = -0.0421(4) °
Preferred orientation parameter:
R_0 = 1.034(1), direction = <0 0 1>
Reliability factors: R_{wp}=8.93%, R_e=5.24%, S=1.70

$Sr_2TMCu_2Te_2O_2$ phases (*TM* = Mn, Co) were also obtained as main phase while small amount of impurity phase such as Cu_7Te_4 and SrTe are observed in each sample including the case of *TM* = Zn as shown in Fig. 1b. The estimated lattice parameters are a = 4.1999(2) Å, 4.1537(4) Å and c = 19.2784(24) Å, 19.5595(37) Å for *TM* = Mn and Co, respectively. Among the known copper oxychalcogenide family $Sr_2TMCu_2Ch_2O_2$ (*Ch* = S, Se, and Te), these Te compounds have the largest *a*- and *c*-axis lattice parameter due to the longer ionic radius of Te compared to those of S and Se,[17-20] consistent with *TM* = Zn compound as mentioned above. In Fig. 1c, while the *c*-axis length of the compounds increases from Mn (19.2784 Å) to Zn (19.5983 Å), *a*-axis length shows the minimum for *TM* = Co. S. G. Tan *et al.*[19] suggested that *a*-axis length directly reflects average ionic radius of *TM* ion whereas *c*-axis length is affected by the amount of Cu deficiency and *Ch*–Cu–*Ch* angle. Assuming that their scenario is correct, since it has the smallest *a*-axis length, ionic radius of Co seems to be smaller than that of Mn and Zn, which has been demonstrated in the previous study on $Sr_2TMCu_2Ch_2O_2$ (*Ch* = S, Se).[12,18,19] On the contrary, different trend is reported in $Sr_2TMAg_2Se_2O_2$,[18] suggesting that complex spin state of this system might lead to the discrepancy between the Cu*Ch* and Ag*Ch* compounds. The compositions were measured by EDX and they were close to ideal values of Sr:TM:Cu:Te=2:1:2:2 considering a few % error of the system (Supplementary Information). The composition of oxygen is not correct because of the formation of hydrated phases and measurement mode with low vacuum.

Figure 2a shows the electronic band structure of $Sr_2ZnCu_2Te_2O_2$ obtained by our first-principles calculation. It shows around 1.7 eV direct band gap at the Γ point. This semiconducting band gap feature is consistent with the results of related compounds such as $Sr_2ZnCu_2S_2O_2$[15,16], though the band gap of the compound is ~1eV larger because of the smaller ionic radii of S than Te. Based on this band structure, power factor (PF) at room temperature and 600 K were estimated using the Boltzmann transport theory as shown in Fig. 2b. PF mainly takes charge of electronic contribution part in thermoelectricity, which is proportional to the thermoelectric performance determined by the figure of merit, $ZT = (PF/\kappa)T = (S^2\sigma/\kappa)T$, where S, σ, κ, and T are the Seebeck coefficient, electrical conductivity, thermal conductivity, and temperature, respectively. In comparison with known thermoelectric compound BiCuSeO, $Sr_2ZnCu_2Te_2O_2$ has a comparable PF around low doping level at both room and high temperature, while it is smaller in heavy doping range. We note that the comparison of PF between $Sr_2ZnCu_2Te_2O_2$ and BiCuSeO presented here is just for reference, because a difference in their relaxation times τ for the electron transport are not taken into account. It is interesting to note that the PF of $Sr_2ZnCu_2Te_2O_2$ shows better performance in the 600 K than 300 K. The origin of this behavior is the splitting of the valence band maxima at the Γ point consisting of the Cu-$d_{xz/yz}$ + Te-*p* orbitals as shown in Fig. 2a. This sizable splitting of around 0.2 eV is induced by SOC because of a large atomic number of Te, which is supported by the fact that the band structure does not exhibit such a splitting when SOC is switched off in the calculation as shown in Fig. 2c. As a result, in Fig. 2b, the PF curve at room temperature shows the double peaks, while they are merged at 600 K where the temperature effect smears the band splitting.

Under the assumption of direct band-to-band transition referring the direct band gap suggested by the first-principles calculation, modified Kubelka-Munk function, $(F(R)h\nu)^2$, versus energy is plotted in Fig. 3. The $F(R)$ is $(1-R)^2/2R$, where the R is reflectance obtained by diffuse reflectance measurement. From the Kubelka-Munk method, band gap size was estimated by extrapolating the slope to $F(R) = 0$ (See dashed lines in Fig. 3). As a result, the Mn and Co compound has ~0.85 and 1.5 eV band gap, respectively. The gap size of Co compound is comparable to the gap ~1.45 eV for isostructural $Sr_2CoCu_2Se_2O_2$[21] and ~1.7 eV suggested by the first-principles calculation for Zn compound, while the relatively small gap is observed in Mn compound. For the Zn compound result, even it is not easy to determine the right absorption edge in the measured energy range.

Overall, electrical conductivity of all the samples harbors a semiconducting behavior as resistivity in Fig. 4a shows. Depending on the *TM* ion, small differences not only in the slope but also in magnitude of the conductivities are observed. Particularly, the Zn compound takes relatively large resistivity than the others for all the temperature range. Since it leads to the lattice parameter change (see Fig. 1d), electrical conductivity can be influenced by *TM* ion substitution in the perovskite layer, although the antifluorite Cu_2Te_2 layer is regarded as the path for charge transportation.

Figure 4b plots the Seebeck coefficient, S, of all the three compounds. Around room temperature, Mn and Co compound shows the largest and smallest S, respectively. Note that S = ~10 VK^{-1} of $Sr_2CoCu_2Te_2O_2$ near room temperature is even much larger than that of isostructural oxyselenide, $Sr_2CoCu_2Se_2O_2$,[21] although the value is the smallest among the present three compounds. For the temperature dependence, S of them exhibits gradual increase with increasing temperature while there is systematic change in slope depending on *TM* element. The slope

tends to become steeper as *TM* element varies from Mn, Zn and Co. As a result, in contrast to the result at low temperature region bellow 450 K, at high temperature above 700 K, the trend changes oppositely as *S* gets larger from Mn, Zn and Co compound. It is interesting to note that *a*-axis lattice parameter shows consistent tendency, since it decreases from Mn, Zn and Co (see Fig. 2d). Considering that in-plane lattice parameter reflects the anion–cation–anion (here, Te–Cu–Te) angle of antifluorite structure and the valence band top consists of Cu 3*d* and Te 5*p* orbitals, change in *a*-axis lattice parameter might influence the electronic structure near Fermi level and *S*, significantly. The possible entanglement of *S* and *a*-axis length highlights that band engineering with variation in *TM* should be an effective way to improve the thermoelectric performance of this perovskite-antifluorite system.

In Fig. 4c, PF of Co compound reaches ~70 $\mu Wm^{-1}K^{-2}$ at 770 K, which is the highest among the three compounds, though it is a couple of times or an order of magnitude lower than that of pristine BiCu*Ch*O (*Ch* = Se, Te), respectively,[10,35,36] and the other typical state-of-the-art thermoelectric materials. Despite having similar *S* at high temperature region, Zn compound shows rather smaller PF because of lower electrical conductivity than Co compound. Sudden changes in slope or anomalies are observed in PF of all the three samples between T = 550 K and 700 K, which attributes to anomalous behavior of resistivity and Seebeck coefficient at the same temperature range. (see Fig. 4a and b, respectively) We repeated the measurements on the same specimen to check whether the anomalies are due to sample decomposition during the temperature sweep. We confirmed that it is reversible with decreasing and increasing temperature, which indicates that it is intrinsic property of $Sr_2TMCu_2Te_2O_2$ compounds.

Thermal conductivity of Mn and Co compounds exhibits similar magnitude and temperature dependence in the overall temperature range including anomalous feature around T = 700 K, while distinct decreasing ratio with temperature reflects the *TM* element dependence as shown in Fig. 5a. The consistent feature between two compounds is plausibly attributed by their identical structure leading to the similar phonon contribution to the heat transportation. With increasing temperature, they get smaller and become ~1.2 W/m·K at the highest measurement temperature ~770 K. It is around three times and 1.5 times larger than that of pristine BiCu*Ch*O (*Ch* = Se, Te),[10,35,36] respectively, while it is still lower than typical materials probably due to the low dimensional structure as well as difference of phonon frequency in oxide and chalcogenide layers. In general, thermal conductivity of so far discovered high thermoelectric materials is smaller than 1 W/m·K, indicating that the two compounds have little bit large thermal conductivity. However, the complex layered structure and the many atoms of variable size in $Sr_2TMCu_2Ch_2O_2$ are still expected to provide opportunities to lower the thermal conductivity, since present study demonstrates the *TM* dependence.

For next, we evaluated figure of merit *ZT* of Mn and Co compounds as shown in Fig. 5b. Rapid increase of *ZT* with increasing temperature from 600 K is observed in Co compound, which reaches ~ 0.045 at around 770 K, while more moderate increase is shown for Mn compound resulting in relatively small $ZT \sim 0.01$. It is interesting to note that although the substitution of *TM* elements (Co and Mn) does not change carrier doping state directly, there is a relatively large difference in *ZT*. This suggests possible new direction of thermoelectricity research with investigating the blocking layer dependence, despite the layer is not thermoelectrically main functional layers. In comparison with the *ZT* of BiCu*Ch*O (*Ch* = Se, Te) which share the Cu_2Ch_2 layer,[10,35,36] *ZT* of the Co compounds remains relatively low about one order but very encouraging considering that this material is not yet optimized but the pristine sample. Significant improvements in thermoelectric response are foreseeable by applying dopant substitution, texturation, and other enhancement methods.[37] For instance, a large improvement in the thermoelectric properties was observed in a previous study with Ba substitution as a strategy to enhance Seebeck coefficient and PF of $Sr_2CoCu_2Se_2O_2$ compound.[21]

It is surprising that the anomalous features in resistivity, Seebeck coefficient, and thermal conductivity appear in the same temperature range between T = 600 and 700 K, which implies that they are presumably correlated with each other. For the origin of the anomalies, structural phase transition can be considered, since the change in structure significantly impacts electron and phonon states which take charge of charge carrier and thermal transportation. Indeed, a lower symmetry with space group C*mca* was reported in $Ba_2ZnAg_2Se_2O_2$[38]. Though XRD patterns of present compounds are well fitted by *I*4/*mmm* model, it cannot be excluded that such small deviation exists in the compounds. If this is the case, one can expect a phase transition from orthorhombic to tetragonal at the temperature. Further investigation is needed to clarify the origin of the anomaly.

On the other hand, regarding the present first-principles band structure calculation result, the valence band splitting owing to SOC can account for the sudden change in the transport properties. As mentioned above, the double peak of PF in Fig. 2b is understood that with increasing hole doping, the participation of higher binding energy split band to the charge carrier transportation becomes significant. In the same frame work, the higher binding energy split band starts to make contribution to the transport mechanism when the temperature is larger than split energy. If latter scenario is the case, the band splitting energy would be smaller than the theoretical suggestion, since converted thermal energy of 600–700 K leading to the anomaly is just around 0.05 eV which is much smaller than the predicted split energy ~0.2 eV. Further study is necessary to resolve this issue.

Figure 6 shows the temperature dependence of the magnetic susceptibility, $\chi(T)$, measured on $Sr_2TMCu_2Te_2O_2$ (*TM* = Mn, Co, Zn). As expected, $Sr_2ZnCu_2Te_2O_2$ harbors a paramagnetic behavior with low magnetization consistent with Zn^{2+} of the main phase being in a fully filled $3d^{10}$ electron state. For $Sr_2CoCu_2Te_2O_2$, a broad hump is observed, which is similar to a reported feature in

$Sr_2CoCu_2Se_2O_2$ compound.[18,19] It has been suggested that the hump is a signature of ordered low dimensional antiferromagnetic (AFM) spin state in CoO_2 sublattice with strong fluctuation. The rapid increase in χ bellow 100K with lowering temperature presumably originates from paramagnetic impurities. On the other hand, $\chi(T)$ of $Sr_2MnCu_2Te_2O_2$ exhibits a sharp peak around 100 K indicating sudden collapse in AFM fluctuation above $T_N \sim 87$ K which is the long-range AFM order transition temperature determined from the maximum position of $d\chi(T)/dT$. The T_N is higher than those of $Sr_2MnCu_2Se_2O_2$ and $Sr_2MnCu_2S_2O_2$, with 54 K and 29.5 K respectively, which is in agreement with the trend suggested by a previous study that T_N increases monotonically with the planar expansion of the MnO_2 layer.[18]

$\chi(T)$ of $Sr_2MnCu_2Te_2O_2$ above 150 K is fitted by Curie-Weiss law, $C/(T-\theta)$, where C and θ are the Curie constant and Weiss temperature, respectively as plotted with red solid line in Fig. 6. The result gives $\theta = 79$ K and the estimated effective magnetic moment, μ_{eff}, of Mn = $5.26\mu_B$ which is slightly smaller than $5.92\mu_B$ that of high-spin d^5 Mn^{2+}. The smaller magnetic moment might be due to presence of Mn^{3+} as previous study pointed out that Cu deficiency exists in the $Sr_2TMCu_2Ch_2O_2$ and it changes the valence of *TM* ion from +2 to +3.[18,19] Indeed, depending on the synthesis condition, Cu_7Te_2 impurity phase easily appears, indicating deficiency of Cu in the main phase. (see Fig. 1c)

Conclusions

To summarize, we successfully synthesized three new layered copper oxytellurides $Sr_2TMCu_2Te_2O_2$ (*TM* = Mn, Co, Zn), as first examples of the compounds with antifluorite Cu_2Te_2 layer and perovskite-like *TM* oxide layer. Reflecting the largest ionic radius of Te among chalcogen elements, it has larger lattice constants than isostructural sulfides and selenides. Depending on the substituted *TM* ion, optical, transport, and magnetic response show significant changes, which highlights the flexibility of the system in tuning the physical properties by substitution of *TM* elements. From the thermoelectric property study, we obtained PF = ~70 $\mu Wm^{-1}K^{-2}$ and $ZT = \sim 0.045$ at 770 K for the Co compound, which encourages further optimization of thermoelectric property to make *ZT* higher. In the magnetism study, the Co and Mn compounds show the signature of AFM order. Present result suggests that replacement of chalcogenide and blocking layer can be a new direction to improve thermoelectric performance of layered copper oxychalcogenides.

Conflicts of interest

There are no conflicts to declare.

Acknowledgements

This study was supported by JSPS KAKENHI Grant Number JP16H06439, JP17H05481, JP16H06441 and JST CREST Grant No. JPMJCR16Q6.

Notes and references

1 H. Kageyama, K. Hayashi, K. Maeda, J. P. Attfield, Z. Hiroi, James M. Rondinelli and K. R. Poeppelmeier, *Nature Communications*, 2018, **9**, 772.
2 Y. Kamihara, H. Hiramatsu, M. Hirano, R. Kawamura, H. Yanagi, T. Kamiya and H. Hosono, *J. Am. Chem. Soc.*, 2006, **128**, 10012.
3 Y. Kamihara, T. Watanabe, M. Hirano and H. Hosono, *J. Am. Chem. Soc.*, 2008, **130**, 3296.
4 Y. Qiu, W. Bao, Q. Huang, T. Yildirim, J. M. Simmons, M. A. Green, J. W. Lynn, Y. C. Gasparovic, J. Li, T. Wu, G. Wu and X. H. Chen, *Phys. Rev. Lett.*, 2008, **101**, 257002.
5 K. Ueda and H. Hosono, J. Appl. Phys., 2002, **91**, 4768.
6 K. Ueda, H. Hosono and N. Hamada, *J. Phys.: Condens. Matter*, 2004, **16**, 5179–5186.
7 K. Ueda, H. Hiramatsu, M. Hirano, T. Kamiya and H. Hosono, *Thin Solid Films, 2006,* **496**, 8 – 15.
8 C. Barreteau, D. Berardan , E. Amzallag, L. D. Zhao and N. Dragoe, *Chem. Mater.*, 2012, **24**, 3168.
9 F. Li, J.-F. Li, L.-D. Zhao, K. Xiang, Y. Liu, B.-P. Zhang, Y.-H. Lin, C.-W. Nana and H.-M. Zhu, *Energy Environ. Sci.*, 2012, **5**, 7188.
10 L.-D. Zhao, J. He, D. Berardan, Y. Lin, J.-F. Li, C.-W. Nan and N. Dragoe, *Energy Environ. Sci.*, 2014, **7**, 2900.
11 H. Ogino, S. Sato, K. Kishio, J.-i. Shimoyama, T. Tohei and Y. Ikuhara, *Appl. Phys. Lett.*, 2010, **97**, 072506.
12 G. R. Stewart, *Rev. Mod. Phys.*, 2011, **83**, 1589.
13 S. Kakiya, K. Kudo, Y. Nishikubo, K. Oku, E. Nishibori, H. Sawa, T. Yamamoto, T. Nozaka, and M. Nohara, *J. Phys. Soc. Jpn.*, 2011, **80**, 093704.
14 E. Brechtel, G. Cordier and H. Schiller, Z. *Naturforsch B*, 1979, **34**, 777.
15 K. Ueda, S. Hirose, H. Kawazoe and H. Hosono, *Chem. Mater.,* 2001, **13**, 1880-1883.
16 H. Hirose, K. Ueda, H. Kawazoe and H. Hosono, *Chem. Mater.*, 2012, **14**, 1037-1041.
17 C. F. Smura, D. R. Parker, M. Zbiri, M. R. Johnson, Z. A. Gál and S. J. Clarke, *J. Am. Chem. Soc.*, 2011, **133**, 2691–2705.
18 S. Jin, X. Chen, J. Guo, M. Lei, J. Lin, J. Xi, W. Wang and W. Wang, *Inorg. Chem.*, 2012, **51,** (19) pp 10185–10192.
19 S.G. Tan, H.C. Lei a, W.J. Lu a, P. Tong, L.J. Li, S. Lin, Y.N. Huang, Z.H. Huang, Y. Liu, B.C. Zhao and Y.P. Sun, *Journal of Alloys and Compounds*, 2014, **598**, 171–176.
20 T. Zhou, Y. Wang, S. Jin, D. Li, X. Lai, T. Ying, H. Zhang, S. Shen, W0 Wang and X. Chen, *Inorg. Chem*., 2014, **53**, 4154−4160.
21 T. L. Chou, O. Mustonen, T. S. Tripathi and M. Karppinen, *J. Phys. Condens. Matter*, 2016, **28**, 035802.
22 D. D. Fan, H. J. Liu, L. Cheng, J. Zhang, P. H. Jiang, J. Wei, J. H. Liang and J. Shi, *Phys. Chem. Chem. Phys*, 2017, **19**, 12913-12920.
23 Dassault Systemes, BIOVIA Corp. Materials Studio Reflex website. http://accelrys.com/products/collaborative-science

/biovia-materials-studio/analytical-and-crystallization-software.html
24 G. Kresse and J. Hafner, *Phys. Rev. B*, 1993, **47**, 558(R).
25 G. Kresse and J. Hafner, *Phys. Rev. B*, 1994, **49**, 14251.
26 G. Kresse and J. Furthmüller, *Comput. Mater. Sci.*, 1996, **6**, 15.
27 G. Kresse and J. Furthmüller, *Phys. Rev. B*, 1996, **54**, 11169.
28 J. P. Perdew, K. Burke and M. Ernzerhof, *Phys. Rev. Lett.*, 1996, **77**, 3865.
29 P. Blaha, K. Schwarz, G. K. H. Madsen, D. Kvasnicka, and J. Luitz, WIEN2k, *An Augmented Plane Wave + Local Orbitals Program for Calculating Crystal Properties*, (Karlheinz Schwarz, Techn. Universität Wien, Austria, 2001).
30 A. D. Becke and E. R. Johnson, *J. Chem. Phys.*, 2006, **124**, 221101.
31 F. Tran and P. Blaha, *Phys. Rev. Lett.*, 2009, **102**, 226401.
32 G. K. H. Madsen and D. J. Singh, *Comput. Phys. Commun.*, 2006, **175**, 67.
33 A. M. Kusainova, P. S. Berdonosov, L. G. Akselrud, L. N. Kholodkovskaya, V. A. Dolgikh and B. A. Popovkin, *J. Solid State Chem.*, 1994, **112**, 189.
34 Y. Liu, J. Lan, W. Xu, Y. Liu, Y.-L. Pei, B. Cheng, D.-B. Liu, Y.-H. Lin and L.-D. Zhao, *Chem. Commun.*, 2013, **49**, 8075.
35 P. Vaqueiro, G. Gúelou, M. Stec, E. Guilmeau and A. V. Powell, *J. Mater. Chem.*, 2013, **A 1**, 520.
36 T.-H. An, Y. S. Lim, H.-S. Choi, W.-S. Seo, C.-H. Park, G.-R. Kim, C. Park, C. H. Lee and J. H. Shim, *J. Mater. Chem. A*, 2014, **2**, 19759.
37 T. Mori, *Small*, 2017, **13**, 1702013.
38 S. J. C. Herkelrath, I. Saratovsky, J. Hadermann and S. J. Clarke, J. Am. Chem. Soc., 2008, **130**, 14426.

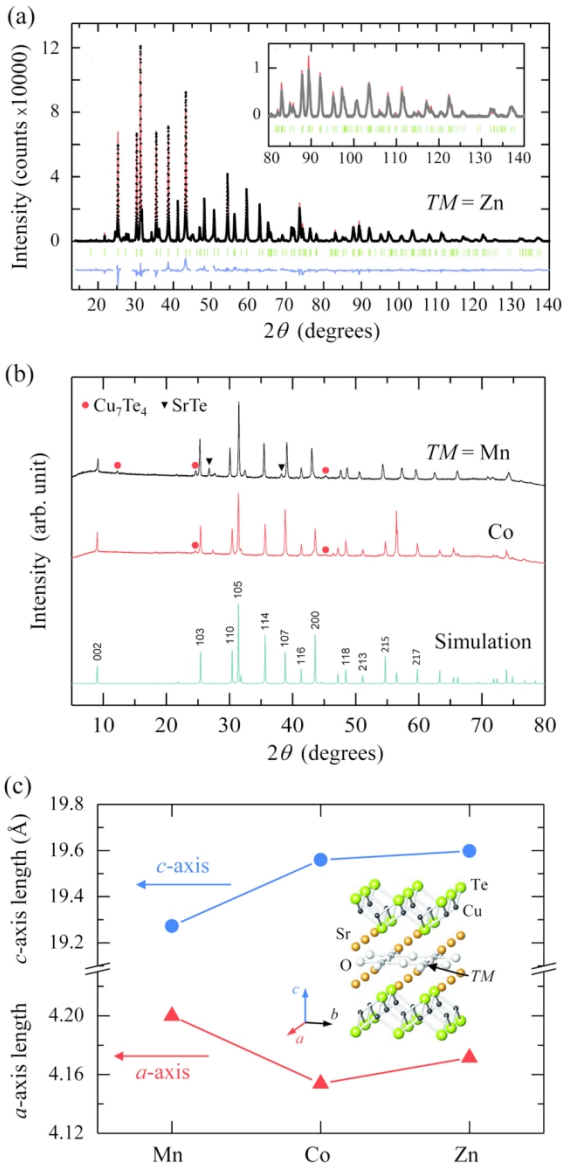

Fig. 1 (a) Rietveld refinement result of $Sr_2ZnCu_2Te_2O_2$ (b) X-ray diffraction patterns of $Sr_2TMCu_2Te_2O_2$ (*TM* = Mn, Co) and simulated pattern of $Sr_2ZnCu_2Te_2O_2$. Red circles and black triangles point peaks from Cu_7Te_4 and SrTe impurity phase, respectively. (c) *TM* ion dependence of *a*- and *c*-axis lattice parameters. Structure of $Sr_2TMCu_2Te_2O_2$ is in (c).

81x160mm (300 x 300 DPI)

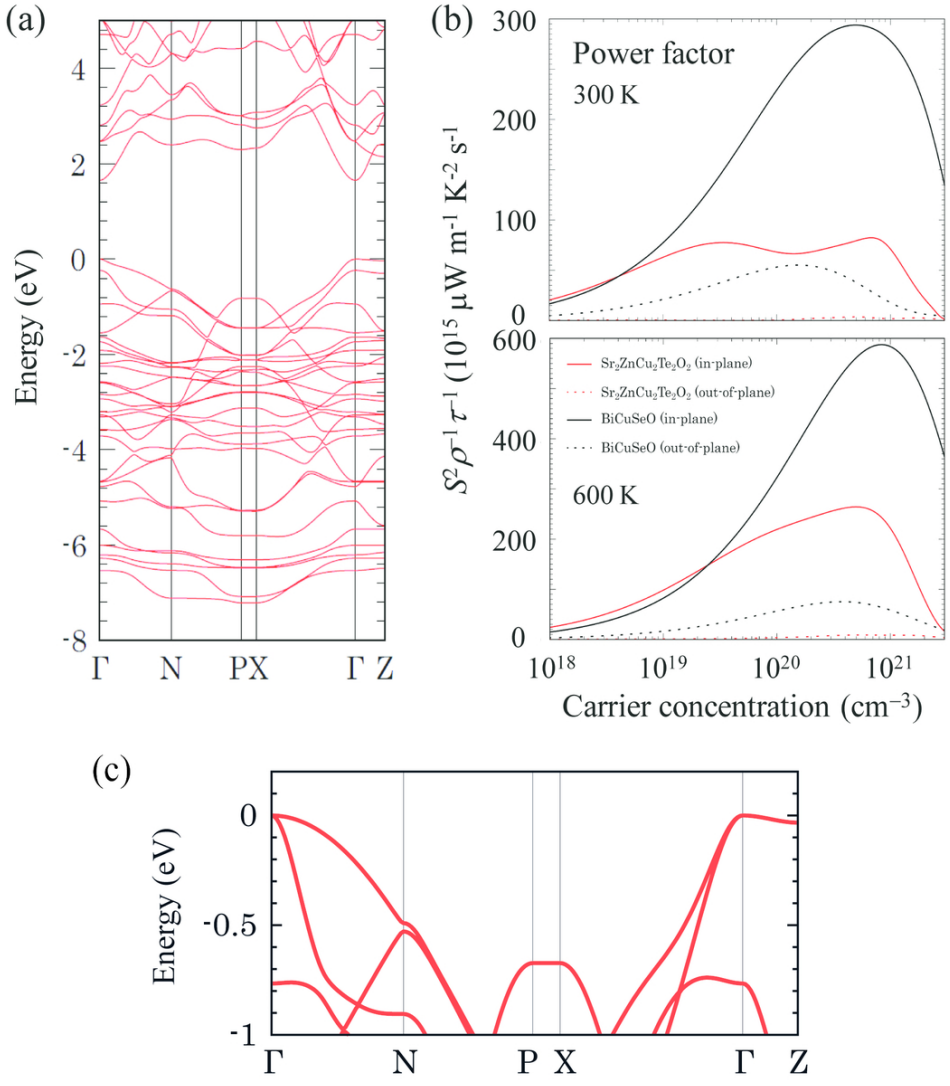

Fig. 2 (a) First-principles band structure of $Sr_2ZnCu_2Te_2O_2$. (b) Power factor (PF) of $Sr_2ZnCu_2Te_2O_2$ at room temperature and 600 K based on the obtained band structure along with PF of BiCuSeO as a reference. (c) Calculated band structure of $Sr_2ZnCu_2Te_2O_2$ near Fermi energy without spin-orbit coupling.

93x105mm (300 x 300 DPI)

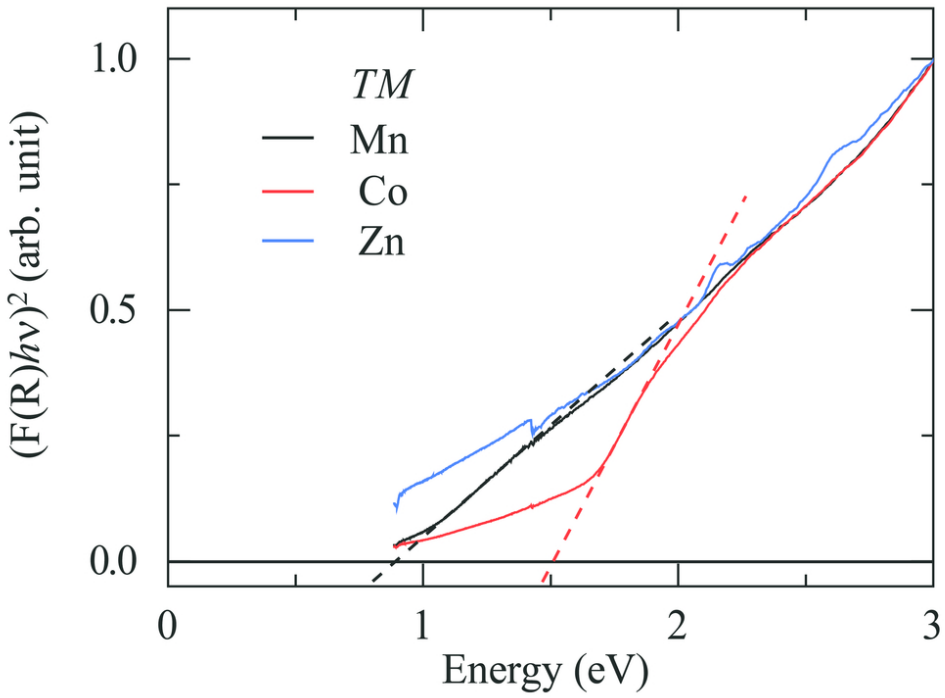

Fig. 3 Modified Kubelka-Munk function, $(F(R)h\nu)^2$, obtained from diffuse reflectance measurements on $Sr_2TMCu_2Te_2O_2$ (*TM* = Mn, Co, Zn). Dashed lines are tangent to the steepest slope of each spectrum.

86x63mm (300 x 300 DPI)

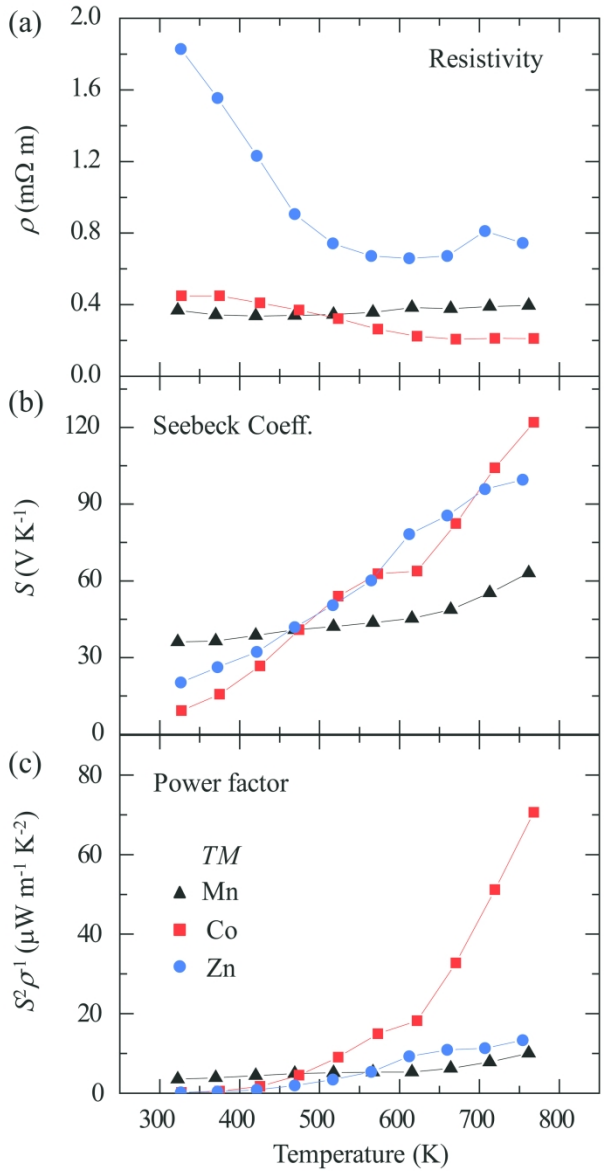

Fig. 4 (a) Resistivity, (b) Seebeck coefficient and (c) PF of $Sr_2TMCu_2Te_2O_2$ (*TM* = Mn, Co, Zn).

225x403mm (300 x 300 DPI)

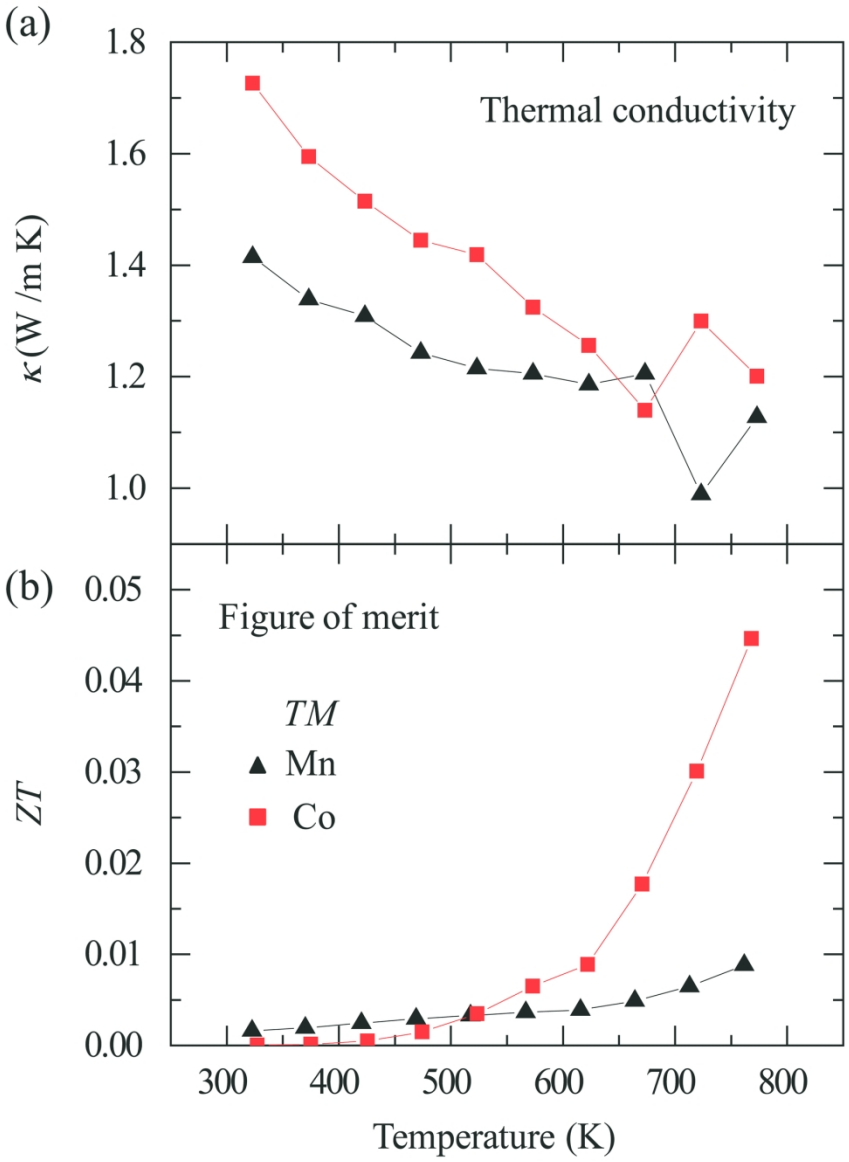

Fig. 5 (a), (b) Thermal conductivity and figure of merit *ZT* of $Sr_2TMCu_2Te_2O_2$ (*TM* = Mn, Co), respectively.

163x209mm (300 x 300 DPI)

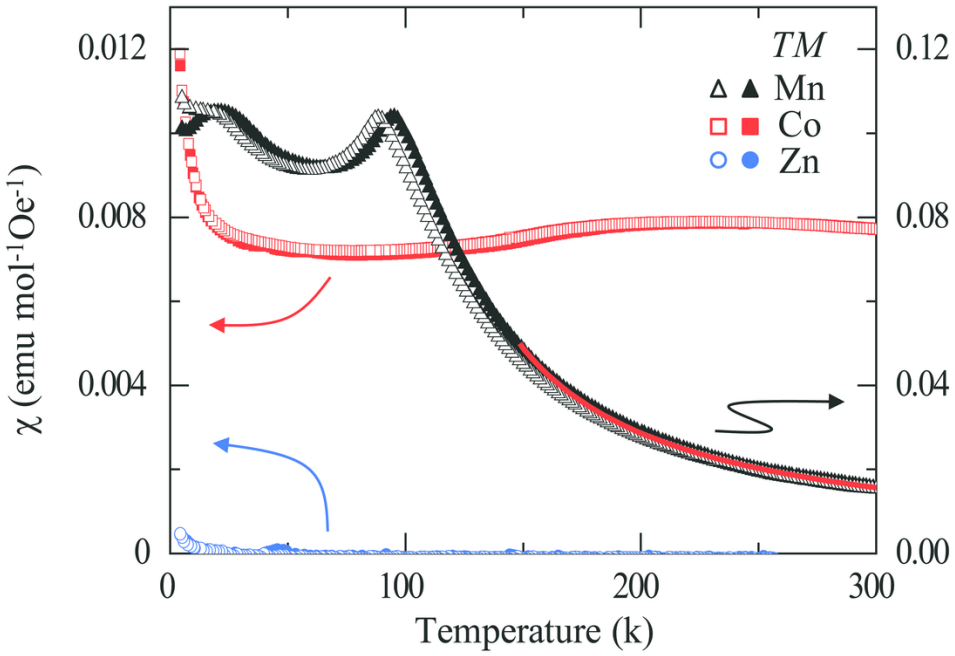

Fig. 6 Temperature dependence of zero-field cool (filled symbol) and field cool (open symbol) magnetic susceptibilities of $Sr_2TMCu_2Te_2O_2$ (*TM* = Mn, Co, Zn) measured at H = 1 kOe. A tiny peak around 50 K in the $Sr_2ZnCu_2Te_2O_2$ data should be an artifact from the frozen oxygen. The fit using the Curie–Weiss law for $Sr_2MnCu_2Te_2O_2$ is shown as a red solid line.

97x69mm (300 x 300 DPI)